Fluid to solid transition in magnetofluidized beds of fine powders

Cite as: J. Appl. Phys. **108**, 054903 (2010); https://doi.org/10.1063/1.3480989
Submitted: 16 December 2009 . Accepted: 21 July 2010 . Published Online: 07 September 2010

J. M. Valverde, M. J. Espin, M. A. S. Quintanilla, and A. Castellanos

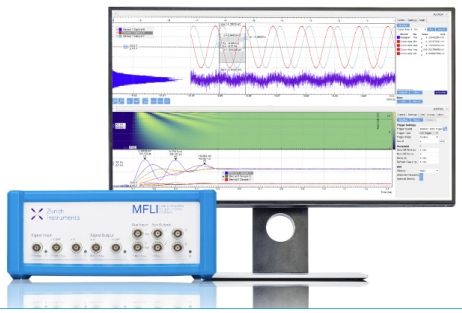

Fluid to solid transition in magnetofluidized beds of fine powders

J. M. Valverde,[1,a)] M. J. Espin,[2] M. A. S. Quintanilla,[1] and A. Castellanos[1]
[1]*Department of Electronics and Electromagnetism, University of Seville, Avenida Reina Mercedes s/n, 41012 Sevilla, Spain*
[2]*Department of Applied Physics II, University of Seville, Avenida Reina Mercedes s/n, 41012 Sevilla, Spain*

(Received 16 December 2009; accepted 21 July 2010; published online 7 September 2010)

Experimental observations on the fluid to solid transition in beds of magnetized fine particles fluidized by gas are reported for different particle sizes (d_p). Contrarily to stability analysis prediction, the fluidized bed is stabilized by a sufficiently strong magnetic field in the cross-flow configuration. As the strength H of the horizontally applied magnetic field is increased, particle chaining in the bubbling bed becomes apparent due to the induced attractive magnetostatic forces between the particles. In close analogy with magnetorheological fluids chain stability is determined by the balance between gas flow shear and the interparticle magnetostatic force. The jamming transition occurs at a gas velocity scaling proportionally to $d_p^2H^2$ when the length of the stable chains reaches a critical size which is independent of particle size. © *2010 American Institute of Physics*. [doi:10.1063/1.3480989]

I. INTRODUCTION

Magnetofluidized beds (MFBs) basically consist of magnetic particles suspended in a vertical gas flow and subjected to a magnetic field. Relevant applications of MFBs can be found in numerous examples such as chemical reactors taking advantage of their high gas-solid contact efficiency or magnetically controlled valves.[1] In general, the flow properties of magnetized particles is a matter of interdisciplinary interest in a wide range of processes and scales besides of MFBs. For example, the flow alignment of magnetic particles is used to identify palaeoflow directions in volcanic rocks and sediments usually in the presence of external fields.[2] Recently, the control of the structuring of magnetizable nanoparticles on a mesoscopic scale has opened a new area of research to achieve structures for a wide variety of applications.[3]

Granular materials are generally characterized by a nonequilibrium kinetic transition from a fluidlike to a solidlike jammed regime.[4,5] At jamming the constituent particles are suddenly arrested in a metastable static state forming a solid disordered network that spans the system. The jamming transition has been described by a phase diagram parametrized by interparticle attractive force, temperature, particle volume fraction, and applied stress.[4] In the case of MFBs, jamming of athermal magnetic particles is driven by the magnetic stress induced by the externally applied magnetic field. Particle size in these systems is usually of the order of tens to hundreds of microns, thus van der Waals forces and Brownian motion are fully negligible. In MFBs particle sedimentation is avoided by subjecting the bed to a countergravity directed gas flow in such a way that the gas pressure drop across the powder balances the material weight per unit area. Fluidized beds are commonly unstable, being characterized by the rapid developments of gas bubbles and large fluctuations of the gas velocity in close analogy with the behavior of sedimenting particle suspensions.[4,6] Gas bubbles can be suppressed in MFBs by the application of a sufficiently strong magnetic field that causes the jamming of the particles. Usually, the field strength needed for jamming is presented as a function of the nondimensional number N_m, defined as the ratio of the solids kinetic energy per unit volume to the magnetic energy. According to Rosensweig stability analysis, based on spatially averaged mass and momentum conservation equations,[1] magnetic stabilization would take place under the condition $N_m N_v < 1$. For magnetically linear solids, $N_v = 4\pi[3-2(1-\phi)]^2(1+\phi\chi_p)/[(1-\phi)^2\phi\cos^2\varphi]$, being ϕ the particle volume fraction, φ the angle between the magnetic field and the direction of the gas flow, and χ_p the particles magnetic susceptibility. As N_v is increased the growth factor of local voidage perturbations is increased. Stability in this continuum model is possible because the magnetic body force arising from gradients of the void fraction smoothes these perturbations. In the case of a cross-flow field ($\varphi=\pi/2$) the value of N_v becomes infinite and magnetic stabilization would not be possible. Yet, experimental observations have evidenced that cross-flow fields are also capable of stabilizing MFBs.[7] Thus, the physical mechanism responsible for the jamming transition in MFBs is far from being fully understood and a widely accepted equation to predict the strength of the field necessary to stabilize MFBs is lacking.

MFBs operated in the cross-flow field configuration bear a close resemblance to magnetorheological fluids (MRFs), in which micron-sized magnetic particles are suspended in nonmagnetic liquids.[8] As in MFBs, particles in MRFs are magnetically multidomain and a magnetic field may induce intense interparticle interactions leading to a transition from a fluidlike to a solidlike regime. Essentially, it can be said that the jamming transition in both MRFs and MFBs is characterized by a common mechanism consisting of the formation of chains of magnetized particles due to the strong magnetostatic interaction induced between them. According to a basic chain model originally developed for MRFs, chain stability

[a)]Electronic mail: jmillan@us.es.

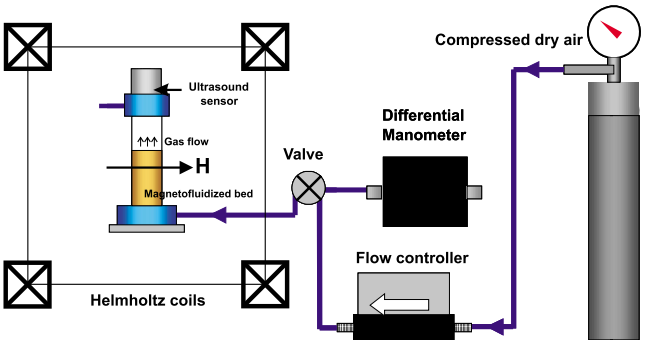

FIG. 1. (Color online) Sketch of the experimental setup used in the magnetofluidization experiments reported in this work.

in MRFs is ruled by the balance between shear and interparticle magnetic forces.[9] We present here an experimental work aimed to look at the jamming transition of MFBs operated in the cross-flow configuration. In close analogy with the behavior of MRFs it will be shown here that a modified chain model is also able to capture the fundamentals of the physical mechanism behind jamming in MFBs.

II. EXPERIMENTAL SETUP

Figure 1 schematizes the experimental setup used in our work. The magnetic powder sample is held in a vertically oriented cylindrical vessel made of polycarbonate ($D=2.54$ cm internal diameter) and rests on a porous plate that acts as gas distributor (5 μm pore size). By means of a mass flow controller (MKS model 1179A, 2000 cm^3/min full scale), a controlled flow of filtered and dried air is pumped through the powder bed while the gas pressure drop Δp across it is read from a differential pressure transducer (MKS model 220CD, 10 Torr full scale). The height of the bed, which gives an average value of the particle volume fraction ϕ, is measured by means of an ultrasonic sensor (Senix model Ultra-S) placed on top of the vessel. This device can determine distance, with an accuracy smaller than local fluctuations in bed height, by sending an ultrasonic wave and measuring the time of reflection from the target. Our magnetic powders have been tested as affected by a horizontal uniform magnetic field externally imposed (cross-flow configuration). This is accomplished by placing the bed in the center of a pair of square Helmholtz coils (50×50 cm), with each coil consisting of 500 turns of 2 mm diameter copper wire. The magnetic field strength H in the close vicinity of the bed is measured by a Hirst magnetics Gauss meter using an axial probe with an accuracy less than 0.1 mT. Experimental measurements show that, within this experimental accuracy, the external field strength is constant in a volume larger than the bed volume.

III. MAGNETIC POWDERS

The magnetic powders used in the experiments consist of magnetite particles of similar permeability but different particle size d_p (35, 50, and 65 μm) artificially made by Xerox Co. and used in practice as carriers of toner particles in the xerographic process. Solid density ρ_p, as measured by means of a AccuPyc 1330 pycnometer, is 5060 kg/m^3. As

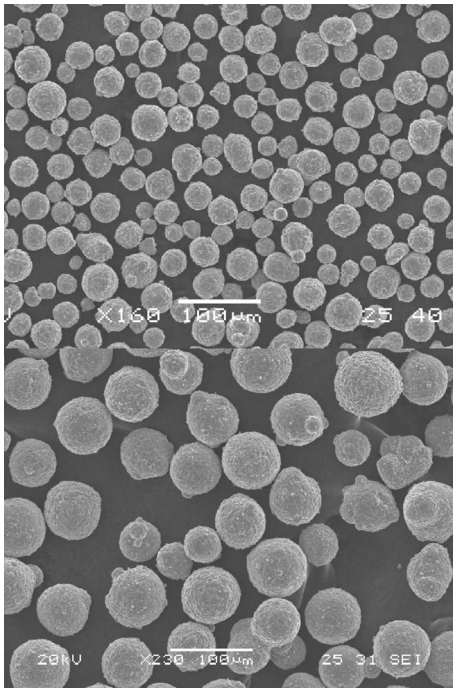

FIG. 2. SEM photograph of 35 μm (top) and 65 μm (bottom) sized magnetite beads used in the experiments.

seen in scanning electron microscopy (SEM) photographs (Fig. 2) these particles are spherically shaped and rather monodisperse.

In the range of field strengths applied ($H<5$ kA/m), the magnetic response of the powders used in our experiments is linear and reversible. This can be observed in Fig. 3, showing experimental data on magnetic characterization of the magnetite powders performed by means of a superconducting quantum interference device (SQUID) magnetometer, where around 1 mg samples were tested. As expected the samples susceptibility χ obtained were similar: $\chi=2.98(d_p=35\ \mu m)$, $2.78(d_p=50\ \mu m)$, and $2.60(d_p=65\ \mu m)$. Accord-

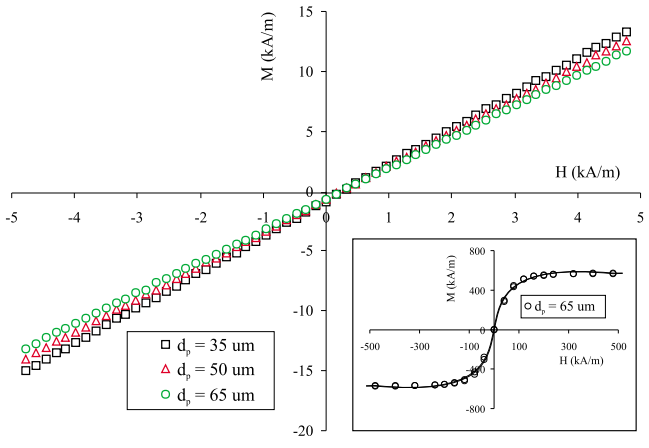

FIG. 3. (Color online) Magnetization of bulk samples of the magnetite powders used in the experiments vs applied field as measured by SQUID magnetometer. The main graph shows the magnetorheological behavior in the interval of field intensities used in our magnetofluidization experiments. The inset shows the magnetorheological behavior in an extended range of field strengths, showing that the magnetization saturates for $H \gtrsim 100$ kA/m.

ing to effective medium theories and numerical analysis on random granular materials,[10] the susceptibility χ of a bed of magnetically linear spherical particles of susceptibility χ_p located in a homogeneous environment of susceptibility χ_0 can be calculated from the Bruggeman mixing rule

$$(1-\phi)\frac{\chi_0-\chi}{3+\chi_0+2\chi}+\phi\frac{\chi_p-\chi}{3+\chi_p+2\chi}=0, \quad (1)$$

where in our case $\chi_0=0$. While the SQUID tests served to check the magnetically linear behavior of the powders tested it is difficult to derive χ_p from these measurements since ϕ cannot be accurately known for the tiny amount of powder samples used. A complementary method employed to obtain χ_p consisted of measuring the change in self-inductance L of a single layer solenoid (number of turns: 300, radius: 41 mm, and length: 16 cm) as the powder was poured into it. In order to measure L we used a precision LCR bridge (model LCR400 Thurlby Thandar Instruments). An advantage of the L-method is that the average particle volume fraction ϕ of the tested samples (of mass about 450 g) filling the inside of the coil could be precisely obtained, which allowed us to estimate χ_p from the averaging Bruggeman equation. The results were: $\chi=2.37$, $\phi=0.425$, $\chi_p=9.52(d_p=35\ \mu\text{m})$; $\chi=2.33$, $\phi=0.417$, $\chi_p=9.72(d_p=50\ \mu\text{m})$; and $\chi=2.42$, $\phi=0.431$, $\chi_p=9.48(d_p=65\ \mu\text{m})$. Hunt *et al.*[11] has reviewed data from the literature reported for magnetite particles of size between 0.01 and 100 μm made from either crushing or crystal growing, which ranged between 2.5 and 10. Thus our results fit in the range of reported values.

IV. EXPERIMENTAL RESULTS

In the experimental procedure the bed is first initialized by subjecting it to a gas velocity large enough to drive it into a bubbling state in which the powder looses memory of previous processes.[12] Once the bed reaches a stationary bubbling regime the horizontal magnetic field is applied. When the magnetic field is applied, the initial gas velocity must be sufficiently large to keep the bed in the bubbling regime. The formation of macroscopic chains at this high gas velocity is thus still offset by the intense hydrodynamic shear. Then the gas velocity v_g is slowly decreased while the gas pressure drop across the bed Δp is measured. Figure 4 illustrates data on Δp versus v_g, showing the effect of the applied field on the behavior of the system. As v_g is slowly decreased and the bed is still in the fluidlike bubbling regime, Δp balances the powder weight per unit area $W\simeq 510$ Pa. However, chaining becomes progressively noticeable in the magnetized bed as evidenced by Fig. 5, which illustrates particle chains elutriated from the MFB. Image samples were obtained by approaching a card of adhesive tape to the free surface. Remarkably, the layer of powder adhered to the tape revealed the presence of chains oriented at a preferential angle $\theta\simeq 60°$ with respect to the direction of the applied field. As a first relevant result these images show that particle chaining does not occur along field lines in the cross-flow MFB. As v_g is further decreased the hydrodynamic shear becomes less intense and at a critical gas velocity $v_g=v_c$ the system is jammed because of the prevailing magnetostatic attractive

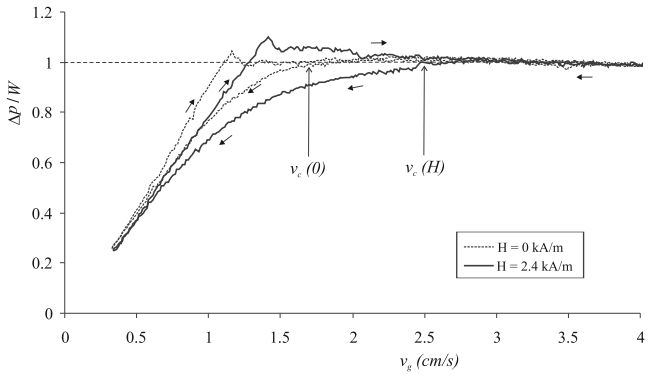

FIG. 4. Gas pressure drop across the powder bed (made nondimensional with the powder weight per unit area W) as a function of gas velocity during the fluidization-defluidization cycles in the absence of magnetic field (top) and presence of a magnetic field (bottom) of strength $H\simeq 2.4$ kA/m. The bed is jammed at $v_g=v_c$, which is indicated.

force between the particles, thus transiting to a solidlike regime. Further decrease in v_g below v_c causes Δp to fall below W since part of the weight is sustained by the enduring network of interparticle contacts in the jammed bed. This allows us to identify v_c from the gas pressure drop measurements. The effect of the field on the jamming transition velocity v_c is seen in Fig. 4, showing that the presence of the field induces jamming at higher gas velocities as the strength of the field is increased. Figure 6 illustrates Δp versus v_g data for fixed field strength and different particle sizes. As can be seen the effect of the field becomes more relevant as particle size is increased. Data of v_c are plotted in Fig. 7 as a function of the magnetic field strength H for the three particle sizes tested (each data point corresponds to an average over around 15 measurements).

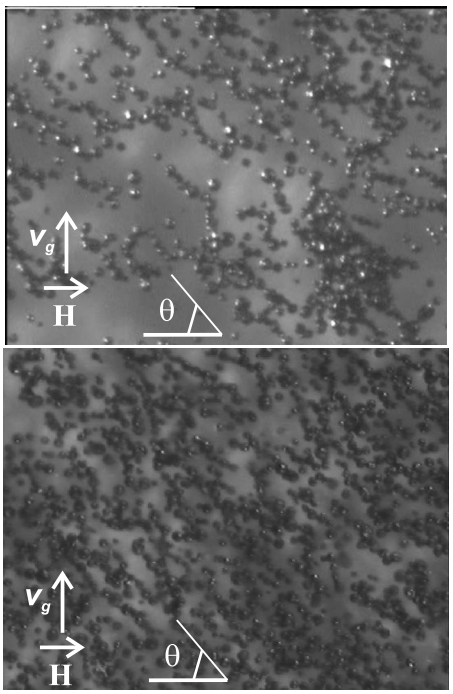

FIG. 5. Optical microscope images of the magnetite particles taken from the bubbling fluidized bed in the presence of a magnetic field. Top: $d_p=35\ \mu$m, $H\simeq 3.2$ kA/m, and $v_g=2$ cm/s. Bottom: $d_p=65\ \mu$m, $H\simeq 5.2$ kA/m, and $v_g=6.6$ cm/s. The angle θ depicted is 60°.

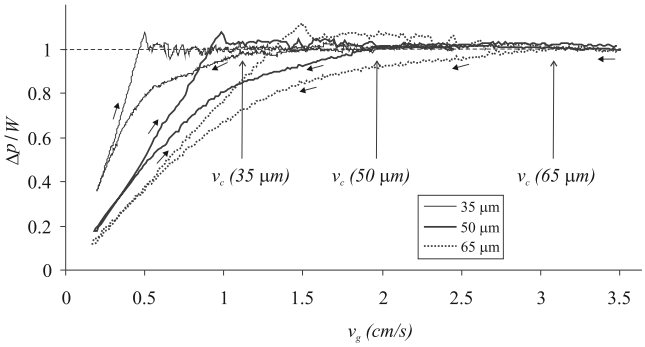

FIG. 6. Gas pressure drop across the powder bed (made nondimensional with the powder weight per unit area W) as a function of gas velocity during the fluidization-defluidization cycles in the presence of a magnetic field of strength $H=2.8$ kA/m. The bed is jammed at $v_g=v_c$, which is indicated.

The effect of the magnetic field on bed expansion is illustrated by Fig. 8, where the particle volume fraction ϕ measured as the gas velocity is decreased from the bubbling regime is plotted against the gas velocity. In the bubbling regime ($v_g > v_c$) the bursting of bubbles at the free surface cause strong fluctuations of bed height, which give rise to strong fluctuations of ϕ. Note however that when the bed is jammed ($v_g \leq v_c$) the intensity of fluctuations is suddenly dropped since bed height remains stable. A remarkable feature revealed by Fig. 8 is that, in the absence of field, ϕ increases as the gas velocity is increased in the bubbling regime ($v_g > v_c$), indicating an increase in the size and frequency of bubbles, which is a well known property of bubbling fluidized beds.[13] In contrast, we observe that, in the presence of a magnetic field, ϕ remains approximately constant in the bubbling regime, which suggests that the particle chains formed are able to limit the growth of gas bubbles. As seen in Figs. 4, Fig. 8 shows that chaining causes the bed to be jammed at higher gas velocities. Moreover, it demonstrates that jamming occurs in states of larger expansion (smaller ϕ). Figure 10 shows data of the particle volume fraction at jamming as a function of the applied field strength. It is observed that, in the absence of field, the bed jams in more open structures as particle size is decreased: $\phi_c \simeq 0.48(d_p=65\ \mu\text{m})$, $0.42(d_p=50\ \mu\text{m})$, and

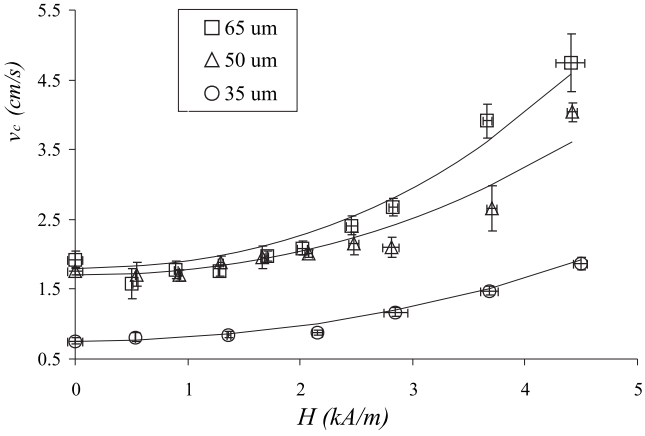

FIG. 7. Gas velocity at jamming transition vs the strength of the magnetic field applied. Solid lines are obtained from Eq. (6) using $L_c \simeq 0.35$ cm as the best fitting parameter for the three particle sizes.

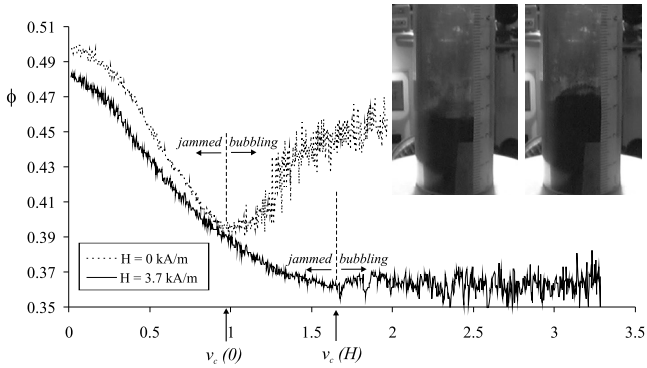

FIG. 8. Particle volume fraction ϕ of the fluidized bed ($d_p=35\ \mu$m) as the gas velocity v_g is decreased from the bubbling regime in the absence of applied magnetic field and in the presence of applied magnetic field of strength $H=3.7$ kA/m. The inset shows snapshots of the jammed bed in the absence (left) and presence (right) of magnetic field.

$0.39(d_p=35\ \mu\text{m})$. This result has been usually reported in the literature.[14] The decrease in particle size implies an increase in natural cohesiveness thus producing relatively looser packed structures. We observe however that as the strength of the field is increased, particle chaining blurs the effect of natural cohesiveness associated to particle size, indicating the progressive prevalence of magnetostatic forces growing with particle size.

V. DISCUSSION

MFBs operated in the cross-flow configuration are similar systems to MRFs. Typically, the suspension of magnetic particles in MRFs is placed between two horizontal plates and a magnetic field **H** is applied in the vertical direction solidifying the structure. The plates are sheared in the horizontal direction at constant shear rate and the force per unit surface needed to initiate flow is defined as the yield stress. Basically, the dynamics of both systems is ruled by the competition between particle chaining induced by the magnetic field and the shear exerted by the fluid essentially in the direction perpendicular to the field. In this section we will show that a chain model originally developed for MRFs can be extended to rationalize the jamming transition in MFBs.

If the ratio of the magnetic permeability of the particles to that of the surrounding fluid ($\alpha=1+\chi_p=\mu_p/\mu_f$) is large, multipolar interactions between the magnetized particles play a relevant role. According to the multipolar expansion, the force between two spheres of diameter d_p linearly magnetized by a field of strength H can be calculated by[15]

$$\mathbf{f}_m = f_m^0 \left(\frac{d_p}{r}\right)^4 [(2f_\parallel \cos^2\theta - f_\perp \sin^2\theta)\hat{u}_r + f_\Gamma \sin 2\theta \hat{u}_\theta]. \tag{2}$$

Here r is the distance between the centers of the two spheres, $f_m^0=(3/16)\pi\mu_f d_p^2 \beta^2 H^2$, where $\beta=(\mu_p-\mu_f)/(\mu_p+2\mu_f)$ and θ is the angle between the chain and the field direction. The force coefficients f_i can be calculated in terms of the multipole moments[15,16] and depend on the magnetic permeability and the distance between the particles. In the dipolar approximation ($r/d_p \to \infty$), $f_i=1$. In the case of two spheres at

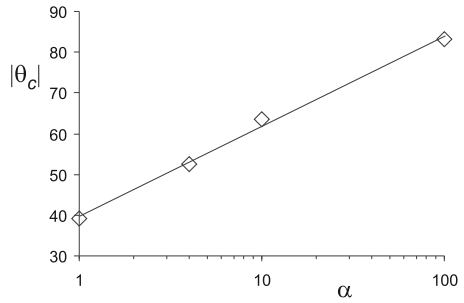

FIG. 9. Critical stability angle of a chain from Eq. (5), and using reported values in the literature for the force coefficients, as a function of the relative permeability of the particles $\alpha=\mu_p/\mu_f$. The solid line is a logarithmic fit to the data.

contact $(r/d_p=1)$ and $\alpha=10$, which approximately corresponds to our case, it is $f_{\parallel}=7.287$, $f_{\perp}=0.6192$, and $f_{\Gamma}=1.5035$.[15] The main effect of increasing the magnetic permeability of the particles is the increase in $f_{\parallel}$, which raises up to $f_{\parallel}=182.21$ for $\alpha=100$, thus further enhancing the attractive interaction.

The mechanical stability of particle chains in MRFs has been analyzed from a chain model based on the balance between the drag force exerted by the shearing fluid on a particle chain and the interparticle magnetostastic force.[9] In our case, particle chains in the bubbling heterogeneous regime are strained by gas velocity fluctuations. A strong fluctuation of the gas velocity will produce on the particle chain a shear force $\mathbf{f}_s$ that opposes the magnetostatic attractive force $\mathbf{f}_m$ between the particles thus limiting the growth of the chain. Let us consider a linear chain of N particles oriented at an angle θ with $\mathbf{H}$. Following the chain model, the angle that the chain makes with the field can be computed by balancing the tangential component of these forces, $\mathbf{f}_m\hat{u}_\theta=\mathbf{f}_s\hat{u}_\theta$. Using the multipolar expansion for the force between spheres at contact [Eq. (2)], this gives

$$\frac{f_s}{f_m^0}=f_\Gamma\frac{\sin 2\theta}{\cos\theta}. \tag{3}$$

Besides, mechanical stability requires that the radial component of $\mathbf{f}_m$ prevails against the radial component of the shear force, $\mathbf{f}_m\hat{u}_r\geq\mathbf{f}_s\hat{u}_r$, or

$$\frac{f_s}{f_m^0}\leq\frac{2f_{\parallel}\cos^2\theta-f_{\perp}\sin^2\theta}{\sin\theta}. \tag{4}$$

By combining Eqs. (3) and (4), the critical stability angle θ_c is obtained as

$$\tan^2\theta_c=\frac{2f_{\parallel}}{2f_{\Gamma}+f_{\perp}}. \tag{5}$$

As can be seen in Fig. 9, where $|\theta_c|$ is plotted as a function of α using reported values of the force coefficients,[15,16] $|\theta_c|$ shows a logarithmic increase with α ($|\theta_c|(^\circ)\simeq\theta_0+9.6\ln\alpha$), where $\theta_0\simeq 39.2^\circ$ corresponds to the dipolar approximation). In our case ($\alpha\simeq 10$) it is $|\theta_c|\simeq 60^\circ$, and it reaches values close to 90° as α approaches $\alpha=100$. Further elaboration of the model should take into account the hydrodynamic interactions between particles in the chain, local field corrections, long range interactions and polydispersity. The effects of these corrections are considered in Ref. 9 for MRFs. Nevertheless it is worth noting that the chain angle observed by us from a bubbling MFB (Fig. 5) is close to the value predicted by the simplest approach. On the other hand, Eq. (5) predicts that the critical stability angle must be independent of gas velocity, particle size, and magnetic field strength. Accordingly, we observe that the orientation of the chains is about the same in pictures obtained for magnetite particles of different particle size, fluidized at different gas velocities and for fields of different strength. A thorough experimental work remains to be performed to confirm these observations. This will be the scope of an independent work in which a noninvasive visualization technique should be also devised. Moreover, the effects of cooperative behavior of the chains or boundary conditions remain also to be addressed.

Let us now calculate the dependence of chain length on field strength, which will serve us to have a deeper insight into the jamming transition. According to experimental observations gas velocity fluctuations in fluidized beds are typically of the order of gas velocity ($\delta v_g\simeq v_g$) and may extend to macroscopic sizes.[17,18] In our MFB chain model the strain on the chain will be thus assumed to be caused by a fluctuation of the gas velocity δv_g extending over the whole length of the chain. We label particles in the chain from 1 to N. Following the chain model, the shear force acting on the particle at the end of the chain will be a sum over contributions from all particles further out in the chain $f_s\simeq\sum_{i=1}^{i=N}3\pi\eta d_p i\Delta v_g$, where Δv_g is the velocity gradient between two contacting particles in the chain ($N\Delta v_g=\delta v_g=v_g$), thus $f_s\simeq 3\pi\eta d_p v_g N/2$. Using Eqs. (3) and (4), the chain length $L_c=Nd_p$ can be thus related to the magnetic field strength H and the gas velocity v_g,

$$L_c\approx\frac{d_p^2}{4\eta v_g}\beta^2\mu_0 H^2 f_\Gamma\sqrt{\frac{2f_{\parallel}}{2f_{\parallel}+2f_{\Gamma}+f_{\perp}}}. \tag{6}$$

It must be taken into account that near jamming, chains are crowded and there will be a strong interaction between the chains which is not accounted for by this simple model of an isolated chain. Furthermore the magnetic field strength within the bulk of the bed H_b will be decreased by demagnetization. Thus, it will be $H_b=H-\kappa M$, where κ is the demagnetization factor ($\kappa=0.5$ for an infinite cylinder magnetized transversely to its axis) and M is the bulk magnetization of the bed. In the case of a linearly magnetizable material $H_b=H/(1+\kappa\chi)$, where $\chi=M/H_b$. Using data on the particle volume fraction at jamming $\phi=\phi_c$ (Fig. 10) and the Bruggeman equation [Eq. (1)], it is obtained that χ shows little variation around $\chi\simeq 2$. Thus, the field strength is decreased within the bulk of the bed by a factor of 0.5 approximately.

In Fig. 7 we plot $v_c=v_c(0)+v_c(H)$, where $v_c(0)$ is the measured gas velocity at jamming in the absence of field and $v_c(H)$ is calculated from Eq. (6), where L_c has been taken as a fitting parameter. The values of the force coefficients used are the values reported for $\alpha=10$ in the literature[16] and demagnetization has been considered by using H_b instead of H in Eq. (6). The same value of $L_c(L_c\simeq 0.35$ cm) gives a good fit to the data for the three particle sizes tested. It must be

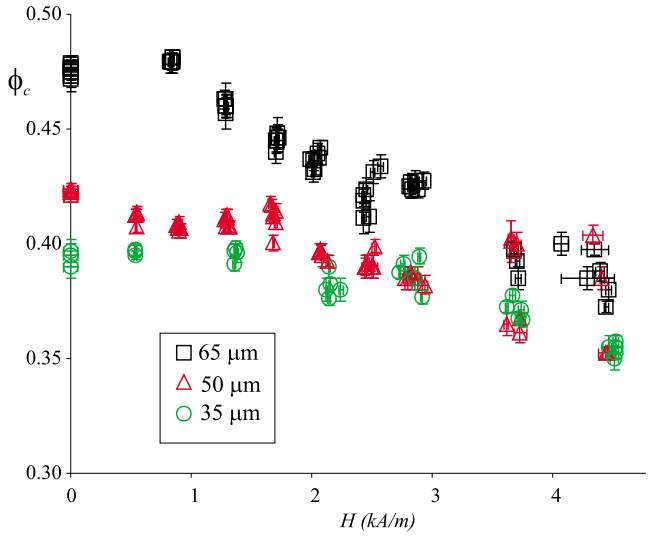

FIG. 10. (Color online) Particle volume fraction ϕ of the fluidized bed at the jamming transition vs the strength of the magnetic field for different particle sizes (indicated).

recognized that a single-chain model is too simple to yield a fully predictive equation even though it is remarkable that a single L_c value serves to fit experimental data independently of particle size. In particular, the interaction between chains near the jamming transition should be considered in a more elaborated analysis. Albeit, the single-chain model proposed in this work is a first step enabling us to rationalize the scaling of the gas velocity at jamming with particle size and field strength observed experimentally.

VI. CONCLUSIONS

In conclusion, we have studied the jamming transition of fluidized beds of magnetic particles as affected by an externally applied cross-flow magnetic field. In close analogy with MRFs, the dynamics of MFBs in the cross-flow configuration is seen to be mainly ruled by the balance between the attractive magnetostatic force between the magnetized particles and the shear force due to the fluidizing gas. As the strength of the magnetic field H is increased, or the gas velocity is decreased, particles tend to chain due to the progressively growing prevalence of the magnetostatic attractive force on the drag force produced on the chains by the gas flow. It has been observed that particle chains are oriented with respect to the applied field at a preferential angle, which according to a chain model based on the balance between magnetostatic and shear forces only depends on the relative magnetic permeability of the particles. Contrarily to the predicted result from stability analysis, it is observed that the MFB may be stabilized by a cross-flow magnetic field. The growth of particle chains as the gas velocity is decreased drives the system to a jamming transition at a critical gas velocity. Experimental data on the gas velocity at jamming are shown to be in accordance with the prediction by a single-chain model when the length of particle chains reaches a critical size which is independent of particle size d_p and showing that the gas velocity at jamming scales proportionally to $d_p^2 H^2$.

ACKNOWLEDGMENTS

This work was supported by Spanish Government Agency Ministerio de Ciencia y Tecnologia (Contract No. FIS2006-03645) and Junta de Andalucia (Contract No. FQM 421).

[1] R. E. Rosensweig, *Ferrohydrodynamics* (Dover, New York, 1997).
[2] D. K. Potter and A. Stephenson, Geophys. Res. Lett. **15**, 1097 (1988).
[3] Y. Lalatonne, J. Richardi, and M. P. Pileni, Nature Mater. **3**, 121 (2004).
[4] P. N. Segrè, E. Herbolzheimer, and P. M. Chaikin, Phys. Rev. Lett. **79**, 2574 (1997).
[5] J. M. Valverde, M. A. S. Quintanilla, and A. Castellanos, Phys. Rev. Lett. **92**, 258303 (2004).
[6] B. Herzhaft and E. Guazelli, J. Fluid Mech. **384**, 133 (1999).
[7] J. Y. Hristov, Powder Technol. **87**, 59 (1996).
[8] T. B. Jones, *Electromechanics of Particles* (Cambridge University Press, Cambridge, 1995).
[9] J. E. Martin and R. A. Anderson, J. Chem. Phys. **104**, 4814 (1996).
[10] K. Karkkainen, A. Sihvola, and K. Nikoskinen, IEEE Trans. Geosci. Remote Sens. **39**, 1013 (2001).
[11] C. P. Hunt, B. M. Moskowitz, and S. K. Banerjee, in *Rocks Physics and Phase Relations: A Handbook of Physical Constants*, edited by T. J. Ahrens (American Geophysical Union, Washington, DC, 1995), pp. 189–204.
[12] J. M. Valverde, A. Castellanos, and M. A. S. Quintanilla, Contemp. Phys. **44**, 389 (2003).
[13] D. Harrison, J. F. Davidson, and J. W. de Kock, Trans. Inst. Chem. Eng. **39**, 202 (1961).
[14] J. M. Valverde and A. Castellanos, Europhys. Lett. **75**, 985 (2006).
[15] D. J. Klingenberg, J. Chem. Phys. **94**, 6170 (1991).
[16] H. Clercx and G. Bossis, Phys. Rev. E **48**, 2721 (1993).
[17] J. M. Valverde, A. Castellanos, and M. A. S. Quintanilla, Phys. Rev. Lett. **86**, 3020 (2001).
[18] J. M. Valverde, M. A. S. Quintanilla, A. Castellanos, and P. Mills, Phys. Rev. E **67**, 016303 (2003).